Nanotechnology **22** (2011) 295713 (5pp) doi:10.1088/0957-4484/22/29/295713

Visualization of spin dynamics in single nanosized magnetic elements

A Banholzer[1,2], R Narkowicz[3], C Hassel[1,4], R Meckenstock[1], S Stienen[1], O Posth[1], D Suter[3], M Farle[1] and J Lindner[1,5]

[1] Faculty of Physics and Center for Nanointegration Duisburg–Essen (CeNIDE), University of Duisburg–Essen, D-47048 Duisburg, Germany
[2] Helmholtz-Zentrum Dresden-Rossendorf, Institute for Ion Beam Physics and Materials Research, D-01328 Dresden, Germany
[3] Department of Physics, Technical University of Dortmund, D-44221 Dortmund, Germany
[4] SMS Siemag AG, Eduard-Schloemann-Straße 4, D-40237 Düsseldorf, Germany

E-mail: juergen.lindner@uni-due.de

Received 12 April 2011, in final form 20 May 2011
Published 21 June 2011
Online at stacks.iop.org/Nano/22/295713

Abstract
The design of future spintronic devices requires a quantitative understanding of the microscopic linear and nonlinear spin relaxation processes governing the magnetization reversal in nanometer-scale ferromagnetic systems. Ferromagnetic resonance is the method of choice for a quantitative analysis of relaxation rates, magnetic anisotropy and susceptibility in a single experiment. The approach offers the possibility of coherent control and manipulation of nanoscaled structures by microwave irradiation. Here, we analyze the different excitation modes in a single nanometer-sized ferromagnetic stripe. Measurements are performed using a microresonator set-up which offers a sensitivity to quantitatively analyze the dynamic and static magnetic properties of single nanomagnets with volumes of $(100\ \mathrm{nm})^3$. Uniform as well as non-uniform volume modes of the spin wave excitation spectrum are identified and found to be in excellent agreement with the results of micromagnetic simulations which allow the visualization of the spatial distribution of these modes in the nanostructures.

(Some figures in this article are in colour only in the electronic version)

1. Introduction

The speed of magnetization reversal in novel spintronic nanoscale devices depends critically on the spin relaxation rates of intrinsic and extrinsic relaxation channels well known in bulk magnets. At the nanoscale, however, these parameters are strongly modified by the surface morphology and shape of the nanostructures. Only by a quantitative understanding of all contributions to magnetic relaxation in nanomagnets (e.g. small particles, hybrid structures or spin-torque nanopillars) can optimized spintronic devices be engineered. Magnetic resonance, i.e. the resonant absorption of microwave radiation by a spin system, has been recognized as one of the best experimental techniques to study the dynamics and statics of spin systems within the ferro-, para- and ferrimagnetic phases, see for example [1, 2]. Results on the exchange coupling between conduction electrons and local magnetic moments, the different spin–spin and spin–orbit contributions to magnetic relaxation and the orbital magnetic moment have been reported as a function of temperature. Different excitation schemes have been employed to study nonlinear effects like magnetic solitons and spin bullets [2, 3] or the spin wave spectrum in nanostructures [4]. In the latter case confinement, which is an inherent property of nanostructures or small devices used in modern applications, leads to drastic changes of the spin wave dispersion [4]. Whenever magnetization dynamics come into play, the spin wave modes are of fundamental importance. In particular the magnetization reversal in small elements such as, for example, spin-torque devices, cannot be correctly described by a macrospin assumption. The excitation of spin waves must be considered, since the magnetization distribution during reversal is non-uniform [5]. Thus, the investigation of such fundamental modes of excitation in magnetic systems

[5] Author to whom any correspondence should be addressed.

at the nanoscale is of high current interest. However, conventional detection schemes which can be applied to all types of magnetic materials offer a sensitivity of the order of 10^{12} electron spins for conventional ferromagnets [6]—not sufficient for the investigation of single nanomagnets. Alternative detection methods like magnetic resonance force microscopy [7], scanning tunneling microscopy [8, 9], optical detection [10–12] or electrical charge detection [13] achieved single spin sensitivity. We have explored the possibility of increasing the sensitivity of the inductive detection using planar microresonators (PMRs) to concentrate the microwave driving fields within small regions. PMRs provide an efficient conversion of microwave power into magnetic field amplitude and, conversely, an efficient conversion of magnetic flux from the precessing magnetization into a propagating electromagnetic field to be detected by the spectrometer. In [14, 15] we explored this potential for the case of paramagnetic samples. Here, we demonstrate that PMRs are well suited for detecting ferromagnetic resonance (FMR) and thus determining magnetic properties like quantization of spin waves in individual nanosized ferromagnetic structures. This unique approach allows—due to its planar on-chip geometry—a straightforward combination with other detection or excitation schemes (e.g. optical, thermal or electrical methods) and is therefore of general interest for investigations of spin dynamics of various material classes at the nanoscale.

2. Experimental procedures

For the fabrication of the PMRs and the Py ($Fe_{30}Ni_{70}$) stripe, we used electron beam lithography. First the microresonator was produced. The protective coating was removed from the 4×4 mm^2 silicon substrate by placing it in an ultrasonic bath with acetone for 10 min, immediately followed by being dried in a nitrogen stream. The backside of the substrate was covered with 5 nm Ti and 10 nm Au in the ultrahigh vacuum (UHV) chamber using electron beam evaporation and with an additional 400 nm Au layer in the HV chamber using thermal evaporation. After an additional cleaning process in acetone, the polymethylmethacrylate photoresist (PMMA) 600K7% was spin-coated onto the front of the substrate. To flatten the resist the substrate was tempered at 150 °C for 10 min. Inside the scanning electron microscope (SEM) the patterns of the PMR and position marks were exposed. Then the resist was developed in 75% methyl isobutyl ketone, 25% isopropanol for 2 min and stopped in an organic solvent for 30 s. In the UHV chamber 5 nm Ti and 10 nm Cu were evaporated. Next, 400 nm Cu and 40 nm Au was deposited in a high vacuum chamber using thermal evaporation as a protective layer. In a 75 °C acetone bath, the remaining resist was removed and the metallized microresonator remained on the substrate. The Py stripe was patterned in a second electron beam lithography processing step. The substrate with the microresonator was spin-coated with the PMMA 950K4% resist and tempered to smooth the surface. Inside the SEM, the substrate was adjusted with the marks in position and the stripe was exposed exactly in the middle of the loop. The resist was developed in the same way as for the microresonator. The 56 nm Py was deposited in the UHV chamber using electron beam evaporation. After a lift-off process the remaining resist and metal was removed and the Py stripe remained. The PMRs were simulated using the finite element method simulation software HFSS (Ansoft). The details on the simulation procedure can be found elsewhere [14, 15]. In order to properly take into account the high-frequency conduction losses in a metallization layer thinner than the skin depth at the resonance frequency, we simulated electromagnetic fields inside the traces. This approach required a very dense mesh within the metallization and is time- and memory-consuming, but delivered quite realistic results. From the simulation, we obtained the dimensions of the PMR, the frequency dependence of the reflection coefficient and the field distribution at the operational frequency.

3. Results and discussion

Figure 1(a) shows schematically the layout of the microresonator. The eigenresonance frequency was chosen to be 14 GHz to match the frequency of the microwave source [14]. By adjusting the design parameters of the microresonator, it is possible to tune its eigenfrequency over a broad frequency range. Figure 1(b) shows an equivalent electric-circuit diagram. The microresonator is based on a microstrip geometry that is coupled to the detection circuit by a coaxial cable. R represents the overall resistance of the microresonator. The capacitor $C1$, given by the rectangular stub, provides impedance matching to the 50 Ω input line. The radial stub, represented by the capacitor $C2$, determines the resonance frequency of the microresonator. The central part of the PMR, the loop, finally provides an inductance L. The microwave magnetic field generated in the PMR is concentrated in the 20 μm loop and oriented perpendicular to the resonator plane, which can be oriented arbitrarily with respect to the static magnetic field.

For demonstration purposes, we chose permalloy, since it is a well-known material with vanishing crystalline anisotropy, so only shape anisotropy has to be considered. Figure 1(c) shows an SEM image of a Py stripe with dimensions 5.04 μm × 0.59 μm × 56 nm, located in the middle of the loop.

Figure 1(d) represents the calculated electric field strength when the resonator is driven at the resonance frequency with an input power of 1 W. The eigenmode corresponds to a standing wave between the rectangular stub and the radial stub, with antinodes at the ends. The length is chosen as half the wavelength of the microwave, taking into account the reduction of the wavelength due to the permittivity of the substrate, which is metallized from the backside. The regions shown in red indicate a high field, while blue represents an almost zero value. Figure 1(e) shows the magnetic field strength inside the loop. At the inner edge of the loop the magnetic field exhibits a maximum and is homogeneous over a large area in the middle of the loop. The microwave efficiency $\Lambda = b_{\mathrm{rf}}/\sqrt{P_{\mathrm{rf}}}$ describing the conversion of microwave power P_{rf} into high-frequency magnetic field amplitude b_{rf} is 30 mT/W$^{1/2}$. This means that a microwave power of 1 W results in a magnetic induction of 30 mT in the center of the loop.

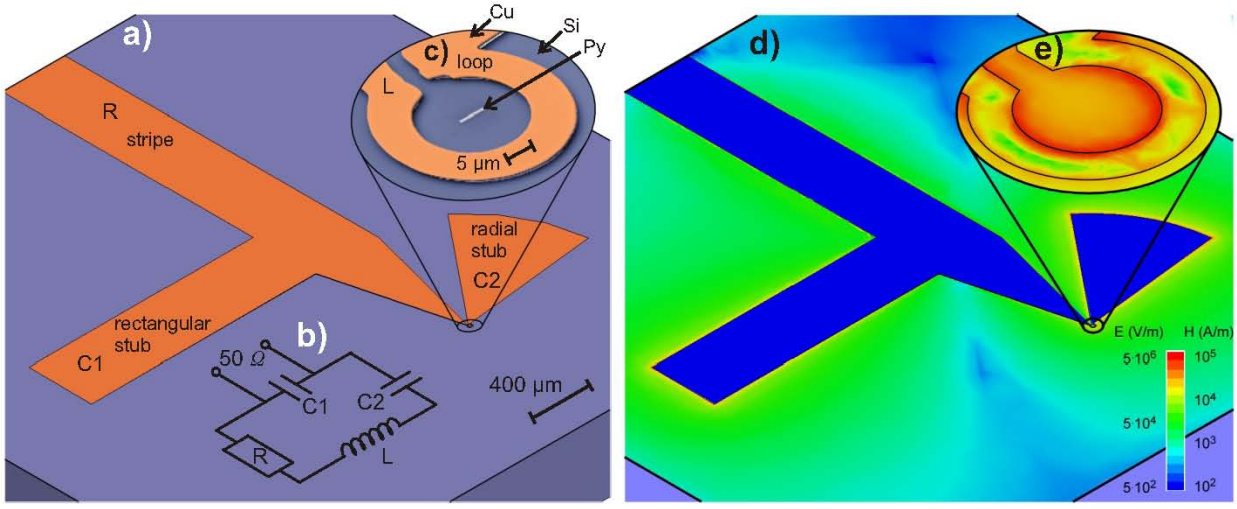

Figure 1. (a) Layout of the microresonator. (b) Equivalent circuit diagram of the microresonator with the capacitors $C1$ and $C2$, the resistance R and the inductance L of the loop. (c) Scanning electron microscope image of the loop of the microresonator with a single permalloy stripe with dimensions of 5.04 μm × 0.59 μm × 56 nm. (d) Simulation of the electric field amplitude of the resonator eigenmode, which forms a standing wave between the ends of the rectangular and the radial stubs. (e) Simulation of the magnetic field inside the loop. The field strengths are calculated for an input power of 1 W. The colour code in (e) and (d) denotes the range of the electric and magnetic field. Blue denotes an electric field (magnetic field) of 5×10^2 V m^{-1} (1×10^2 A m^{-1}), while red refers to an electric field (magnetic field) of 5×10^5 V m^{-1} (1×10^5 A m^{-1}).

For the FMR measurements described here, a static magnetic field $\vec{B}_{\text{ext}}$ is applied in the resonator plane, perpendicular to the long axis of the stripe. Figure 2(a) shows the observed FMR spectrum as a function of the static magnetic field at a microwave power of 0.2 mW. Clearly observable are five different resonance signals. To get an insight into the origin of these modes, we simulated the system, using the software package OOMMF [16]. For these simulations, the exact geometry of the stripe was used, as measured by SEM. The crystalline anisotropy was set to zero, the magnetization $M = 830$ kA m^{-1} as determined from SQUID measurements and an exchange constant of $A = 13 \times 10^{-12}$ J m^{-1} was assumed [17]. The high-frequency magnetic field was considered to be perpendicular to the substrate. Figure 2(b) shows the result of the OOMMF simulation, where the derivative of the dynamic component of the magnetization pointing out of the plane (z direction) is plotted versus the applied magnetic field. Note that this quantity is proportional to the derivative of the imaginary part of the high-frequency susceptibility component $\partial\chi''/\partial B$ along the z direction. In this simulation, the same five signals as in the experiment are observed.

The largest signal with index 4 is the uniform mode of the Py stripe, where all magnetic moments of the sample precess in phase. Besides the spectra, the OOMMF simulations also provide 'snapshots' of the precessing magnetization. Figure 3(a) shows the z component of the magnetization as blue/white/red contrast, whereby blue (red) denotes the magnetization pointing out of (into) the film plane, while white denotes a magnetization lying in the film plane. The images are numbered to allow correlation with the spectra shown in figure 2. For the uniform mode (no. 4) the whole area inside the stripe is homogeneously blue, indicating that a z component of the magnetization due to the FMR exists. The amplitude gradually decreases toward the edges of the sample.

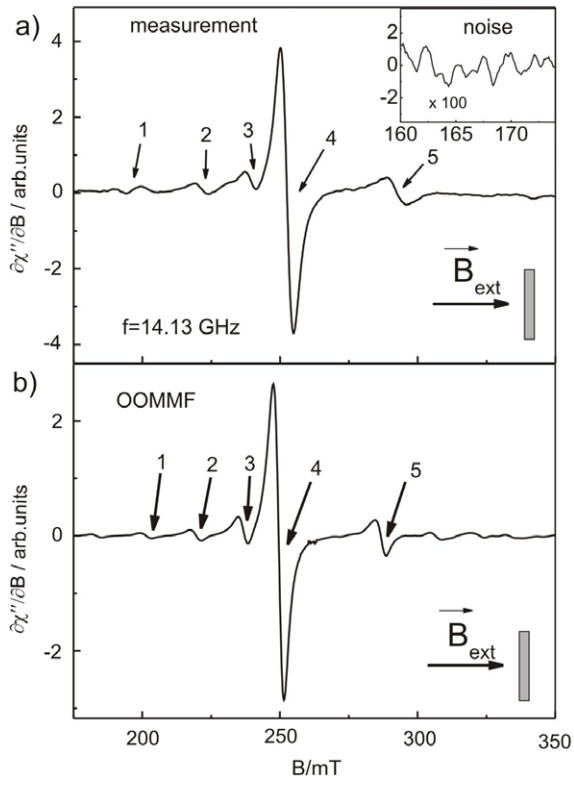

Figure 2. (a) Room temperature FMR measurement at 14.13 GHz and a microwave power of 0.2 mW. (b) OOMMF simulation of the Py stripe at a frequency of 14.13 GHz. The FMR signals are numbered from one to five and can be related to the OOMMF simulations and sketches in figure 3. The uniform excitation is marked as no. 4. The other signals correspond to standing spin waves.

The three signals at lower fields are spin wave modes with standing wave character. These modes can be observed in structures with finite sizes only, where propagating spin

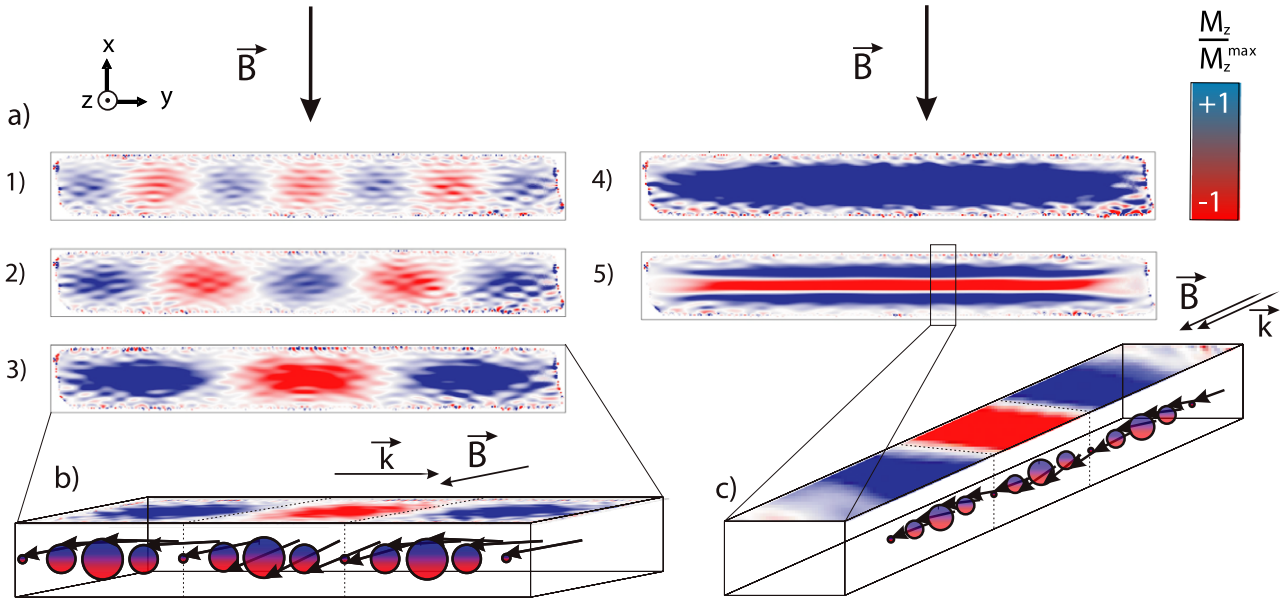

Figure 3. OOMMF simulation of the spin configuration of the Py stripe shown in figure 1(b) in the microresonator while in resonance. In the blue areas, the spins point out of the plane of projection and in the red areas into it. (a) Simulated z components of the spins in the stripe at the resonance fields marked with numbers 1–5. The external magnetic field $\vec{B}_{\text{ext}}$ is perpendicular to the long side of the stripe. (b) Three-dimensional sketch of mode number 3 with the spin configuration shown on top. The arrows indicate the magnetization components. Note that the color code denotes the out-of-plane component of the dynamic magnetization in z direction (see also legend). (c) Same for mode no. 5.

wave modes are reflected at the edges of the sample. Since these spin wave modes are located at lower fields than the uniform mode, they have a higher excitation energy. Thus, one can conclude, that the propagation direction in this case is oriented perpendicular to the magnetic field direction [2]. This conclusion is again supported by the OOMMF simulation 'snapshots' shown in figure 3(a). Each of the modes with numbers 1–3 contains an odd number of antinodes where the magnetization is pointing out of the film plane (blue) and into the film plane (red). Between those regions there are areas where no out-of-plane component is present. The corresponding magnetization configuration is schematically shown in figure 3(b) for mode no. 3. The main (static) part of the magnetization is aligned parallel to the external magnetic field. Additionally, there is a small component of the precessing magnetization due to the applied microwave field. The higher energy of the mode with respect to the uniform mode results from the contribution of the dipole–dipole interaction between the dynamic magnetization components [2].

Also mode no. 5 can be identified as a standing spin wave mode with the wavevector parallel to the magnetic field direction. The OOMMF 'snapshot' of this mode is shown in figure 3(c). The structure of the red/blue contrast is rotated by 90° as compared to figure 3(b). It can be seen that the main direction of the magnetization and the wavevector are in this case parallel. In this spin wave mode, the dipolar contribution reduces the energy compared to the uniform mode [2]. Since the wavelength is reduced compared to the case where the wavevector is oriented in the direction of the long axis of the stripe, a larger shift of mode no. 5 away from the uniform mode results when compared to modes 1–3. The observed signals are thus identified as different spin wave modes, in very good agreement with theoretical simulations. Table 1 compares the experimental magnetic field values of the different resonances with the corresponding theoretical values, which gives a maximum difference between theory and experiment of only 2.2%.

Table 1. Resonance fields of the resonance modes indicated in figure 2 in the measurement and the OOMMF simulation.

B_{res}, mT:	(1)	(2)	(3)	(4)	(5)
Measurement	203	222	240	252.5	293
Simulation	201.4	219.6	237	249.6	286.6
Difference (%)	0.8	1.1	1.3	1.1	2.2

4. Estimate of performance

The measured stripe exhibits a total magnetic moment of $\mu_{\text{T}} = 1.48 \times 10^{10}\ \mu_{\text{B}}$ (μ_{B} is the Bohr magneton), which can easily be detected by the set-up (signal-to-noise ratio of about 300:1). The PMR method is thus capable of detecting signals of single ferromagnetic specimens with edge lengths of 100 nm.

The magnetic resonance signal, generated in the loop of the PMR by the precessing magnetic moment of the sample, is defined by the value of the magnetic moment μ_{T}, the frequency of operation ω and the coupling between the magnetic moment and the loop of the PMR: $S \propto \omega\mu_{\text{T}}\Lambda$. The coupling is determined by the microwave efficiency Λ of the PMR. This is the only parameter that depends on the dimensions of the PMR. To extrapolate the sensitivity of the PMR down

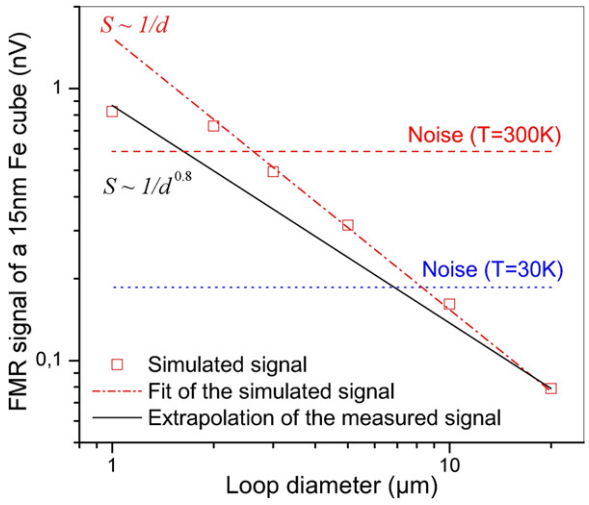

Figure 4. FMR signal amplitude at the receiver input, normalized to the magnetic moment of a single 15 nm Fe cube, as a function of the loop diameter at room temperature. The open squares stand for the signal values, calculated from the scaling of the microwave efficiency. The dashed–dotted line represents a linear fit to the simulated data, while the solid line is a power function $S \propto 1/d^{0.8}$, resulting from our previous measurements. The horizontal dashed and dotted lines mark the (theoretical) thermal noise level of a 50 Ω resistor at 300 K and 30 K, respectively.

to the loop diameters of about 1 μm, we simulated the microwave efficiency of the PMRs, scaling the loop trace width proportionally to the diameter d. The microwave efficiency was obtained from the microwave magnetic field value in the center of the loop. In a simulation both the microwave efficiency and the signal induced in the PMR scale linearly with the inverse loop diameter down to 2 μm (open squares in figure 4). At the diameter of 1 μm saturation of the signal growth with inverse loop diameter is observed. The trace width is scaled proportionally to the diameter down to 0.5 μm, which is less than the skin depth in a golden trace at 14 GHz (0.66 μm). This causes strong resistive losses due to the skin effect and limits the expected increase of the microwave efficiency and the FMR signal. To solve this issue, one would have to cool the PMR down to about 30 K. At 30 K the skin depth of gold is about 0.12 μm, so we can reduce the trace width down to 0.5 μm and the loop diameter to 1 μm without significant increase of the resistive losses. In our measurements of the PMRs with the loop diameters from 500 to 20 μm we found that the detected signal scales as $S \propto 1/d^{0.8}$ [15]. Thus, scaling of the signal with the inverse loop diameter is slightly less steep than linear. Nevertheless both extrapolations predict that the signal of an Fe cube with 15 nm edge length (magnetic moments of $\mu = 6.19 \times 10^5 \mu_B$) in the PMR with a loop diameter of 1 μm should be clearly above the thermal noise level. The sensitivity could be even higher if the resonance linewidth decreases, which is expected for single-crystalline materials [18].

5. Conclusions

Our results demonstrate that PMRs enable direct investigation of the dynamic magnetic properties of single nanomagnets allowing for the observation of spin wave modes unique to nanoscale structures. This approach is applicable to a vast variety of magnetic materials and can be combined with optical, electrical and thermal excitation and detection techniques.

References

[1] Farle M 1998 *Rep. Prog. Phys.* **61** 755
[2] Patton C E 1983 *Phys. Rep.* **103** 251
[3] Slavin A N, Demokritov S O and Hillebrands B 2002 *Spin Dynamics in Confined Magnetic Structures I* (*Topics Appl. Physics*) vol 83, ed B Hillebrands and K Ounadjela (Berlin: Springer) pp 35–65
[4] Stiles M D and Miltat J 2006 *Spin Dynamics in Confined Magnetic Structures III* (*Topics Appl. Physics*) vol 101, ed B Hillebrands and A Thiaville (Berlin: Springer) pp 225–308
[5] Demokritov S O and Hillebrands B 2002 *Spin Dynamics in Confined Magnetic Structures I* (*Topics Appl. Physics*) vol 83, ed B Hillebrands and K Ounadjela (Berlin: Springer) pp 65–93
[6] Poole C P 1983 *Electron Spin Resonance, A Comprehensive Treatise on Experimental Technique* (New York: Wiley)
[7] Rugar D, Budakian R, Mamin H J and Chui B W 2004 *Nature* **430** 329
[8] Manassen Y, Hamers R J, Demuth J E and Castellano A J Jr 1989 *Phys. Rev. Lett.* **62** 2531
[9] Durkan C and Welland M E 2002 *Appl. Phys. Lett.* **80** 458
[10] Wrachtrup J, von Borczyskowski C, Bernard J, Orrit M and Brown R 1993 *Nature* **363** 244
[11] Gruber A, Dräbenstedt A, Tietz C, Fleury L, Wrachtrup J and von Borczyskowski C 1997 *Science* **276** 2012
[12] Köhler J, Disselhorst J A J M, Donckers M C J M, Groenen E J J, Schmidt J and Moerner W E 1993 *Nature* **363** 242
[13] Xiao M, Martin I, Yablonovitch E and Jiang H W 2004 *Nature* **430** 435
[14] Narkowicz R, Suter D and Stonies R 2005 *J. Magn. Reson.* **175** 275
[15] Narkowicz R, Suter D and Niemeyer I 2008 *Rev. Sci. Instrum.* **79** 084702
[16] http://math.nist.gov/oommf/
[17] Vavassori P, Grimsditch M, Novosad V, Metlushko V and Ilic B 2003 *Phys. Rev.* B **67** 134429
[18] Lindner J and Farle M 2008 *Magnetic Heterostructures—Advances and Perspectives in Spinstructures and Spintransport* (*Springer Tracts in Modern Physics*) vol 227 (Berlin: Springer) pp 45–96

Visualization of spin dynamics in single nanosized magnetic elements

2011 Nanotechnology 22 295713

(http://iopscience.iop.org/0957-4484/22/29/295713)